Applications in Energy and Combustion Science 12 (2022) 100090

Contents lists available at ScienceDirect

Applications in Energy and Combustion Science

journal homepage: www.sciencedirect.com/journal/applications-in-energy-and-combustion-science

# Comparison of properties of biochar produced from different types of lignocellulosic biomass by slow pyrolysis at 600 °C

Liang Wang [a,*], Maria N.P. Olsen [a], Christophe Moni [b], Alba Dieguez-Alonso [c], José María de la Rosa [d], Marianne Stenrød [b], Xingang Liu [e], Liangang Mao [e]

[a] SINTEF Energy Research, P.O. Box 4761 Torgarden, NO-7465 Trondheim, Norway
[b] Norwegian Institute of Bioeconomy Research (NIBIO), Høgskoleveien 7, 1433 Aas, Norway
[c] Institute of Fluid Dynamics and Thermodynamics, Faculty of Process and Systems Engineering, Otto von Guericke University Magdeburg, Universitätsplatz 2, DE-39106 Magdeburg, Germany
[d] Instituto de Recursos Naturales y Agrobiología de Sevilla (IRNAS-CSIC), Reina Mercedes Av. 10, 41012, Seville, Spain
[e] State Key Laboratory for Biology of Plant Disease and Insect Pests, Institute of Plant Protection, Chinese Academy of Agricultural Sciences, Beijing 100193, China

ARTICLE INFO

*Keywords:*
Corn cob
Corn stalk
Spruce wood
Biochar
Pyrolysis
Properties

ABSTRACT

Production of biochar from corn cob and corn stalk has gained great interest for efficient waste management with benefits of improving soil properties, increasing crop productivity, and contributing to carbon sequestration. This study investigated slow pyrolysis of corn cob and corn stalk at 600 °C to characterize yields and properties of products, with focus on solid biochar. Spruce wood, a rather well studied woody biomass, was also included for comparison purposes. It was observed that yields of biochar and condensates from corn cob, corn stalk, and spruce wood were comparable. However, gas release profiles and yields from the three biomasses were quite different, which is mainly related to the different chemical compositions (i.e., hemicellulose, cellulose, lignin, and inorganic species) of the studied raw feedstocks. The produced biochars were analyzed for proximate analysis, CHNS-elemental analysis, specific surface area and specific pore volume for pores in the nm-range, inorganic composition, solid functional groups, and aromaticity. The corn cob and corn stalk biochar presented significantly higher concentration of inorganic elements, especially P and K, favoring soil application. The SEM analysis results showed that the spruce wood biochar has different microstructure than corn cob and corn stalk biochars. Condensates and light gases, as by-products from biochar production, contained over 50% of the energy and 40% of the total carbon of the initial biomass. Utilization of the condensates and light gases as valuable resources is therefore critical for improving environmental and energy benefits of the biochar production process.

## 1. Introduction

Corn is one of the most ubiquitous and extensively planted crops in the world. Global production for 2019/2020 was 1,116.41 million metric tons and is expected to be 1,133.89 million metric tons for 2020/2021, with an increase of 17.47 million tons or 1.57% in corn production around the globe [1]. The top three producers, U.S., China, and Brazil, account for over 65% of the global production. In China alone, the yield of corn was 260,670,000 t in 2021. The ratio between corn grain and corncob (CC) can be around 100:18, which means approximately $3.7 \times 10^7$ t CC could be generated in China only [1]. CC is collected and transported for further processing, which is a main mass stream after separation from corn grain. Only small fractions of generated CC are now used as a raw material for few industrial processes [2]. Significant amounts of CC are still employed as feedstock in making low-grade fuels and products or even burned directly in many parts of the world. Corn stalk (CS) is a main residue after harvesting of corn, which is usually kept in the farmlands [3]. Considering the large amounts of CC and CS produced each year, attempts have been made to exploit these agricultural wastes and convert them to different products [3–6]. However, bottlenecks remain in efficient and economical conversion of them into desired products. There are evident need to identify and assess measures and technologies for proper processing and utilization of CC and CC to yield valuable products.

Different thermochemical conversion processes have been developed to produce biochar/carbonaceous residue from biomass, including

* Corresponding author.

https://doi.org/10.1016/j.jaecs.2022.100090
Received 4 January 2022; Received in revised form 16 June 2022; Accepted 4 October 2022
Available online 5 October 2022
2666-352X/© 2022 The Authors. Published by Elsevier Ltd. This is an open access article under the CC BY license (http://creativecommons.org/licenses/by/4.0/).

torrefaction, pyrolysis and carbonization. Slow pyrolysis is currently the most applied technology aiming to produce carbonaceous solid product biochar with the possibility to alter biochar property through altering process conditions [5,3,10]. Upon slow pyrolysis, degradation, decomposition, and conversion of biomass occur with the formation of a carbon rich solid, as well as condensable and non-condensable volatile products [6,7]. To optimize the biochar production, slow pyrolysis is commonly applied to thermally convert biomass feedstock in a broad temperature range from 300 to 800 °C, with a slow heating rate from 1 to 20 °C/min and residence times from hours to days. The biochar is a porous, carbon rich material that has unique chemical, physical, and biological properties [8]. The condensable volatile products generated during biochar production can be condensed into liquid bio-oil. The bio-oil mainly consists of organic and aqueous phases and can be used as an energy vector or further upgraded into valuable chemicals [9]. The non-condensable volatiles include light non-condensable hydrocarbons, carbon dioxide, carbon monoxide, hydrogen, and methane. Biochar has gained increasing interest and recognition as an efficient material for versatile applications, including soil amendment, climate change mitigation, environmental remediation, and functional materials production for different industrial applications [10]. However, previous studies on biochar production and application are mainly focused on woody biomasses and certain crop residues [17–19]. There is a clear need to evaluate the formation mechanisms and physicochemical characteristics of biochars from other interesting agricultural residues such as CC and CS.

Several factors significantly impact the conversion behavior of biomass, and therefore yields and characteristics of biochar, bio-oil, and non-condensable gases produced during pyrolysis processes [11]. The characteristics and quality of biochar are critical for selecting the strategy to upgrade and modify the targeted biochar properties and determine its performance for a certain application. Feedstock type is among the most influential factors that affect the final characteristics of the biochar [6]. Biomass is biologically formed mainly by cellulose, hemicellulose, and lignin. The overall composition varies significantly among different biomass types, as well as within a single feedstock category [12]. This variation is even higher for herbaceous feedstocks. It has been reported that cellulose, hemicellulose, and lignin content of woody biomasses can be 51.2%, 21.0% and 26.1%, respectively [12]. Whereas contents of these three main components in herbaceous biomasses have been reported to be 32.1%, 18.6% and 16.3%, respectively [13]. During the pyrolysis process cellulose, hemicellulose, and lignin decompose in specific ranges of temperature through very complex reaction mechanisms [13], which considerably affect determine the carbonaceous structure and physicochemical properties of the produced biochar [14,15]. Pyrolysis of biomass with a high lignin content tends to produce biochar with a high fixed carbon content, high specific surface area, and a more stable aromatic structure [11]. Furthermore, biomass contains diverse inorganic elements that remain in biochar in different chemical states upon the pyrolysis process. The presence of these inorganic elements can considerably influence the biomass conversion and bestow functionalities and hence potential applications of the produced biochar. Several studies stated that biochar derived from herbaceous biomass materials have significantly higher content of inorganic elements than that of biochar derived from woody biomasses [11,13,14]. It consequently affects key properties of biochar, such as pH, nutrient availability, and surface charges, as well as further functionality and performance of the biochar. Apart from the characteristics of the feedstock, conversion of biomass and product distribution and composition are considerably affected by production conditions, mainly process temperature and residence time [5,3,10], resulting in biochars with different structures and physiochemical properties [10]. Typical temperatures for slow pyrolysis are in the range of 400–700 °C. Biomass pyrolysis at higher temperatures yields biochar with higher specific surface area, pH value, ash and carbon content. Other relevant biochar properties also change upon different pyrolysis temperature, including amount and type of surface functional groups, alkalinity, and stability, which are critical for biochar as soil stimulator and sorbent for contaminants management [20]. Therefore, selection of appropriate temperature is often a trade-off between yield, physiochemical properties, and functional characteristics of the biochar [7].

Production and application of biochar have been shown as a promising way to manage agricultural waste with benefits to improve soil properties, enhance crop yield, and remediate environmental issues. Corn cob and corn stalk are non-edible agricultural residues from corn production. Utilization of CC and CS for production of biochar does not compete or interfere with food production. Biochar production enables the conversion of waste CC and CS into value-added products and the realization of smart recycling of materials and nutrients in a circular bio-based economy. The existing literature has primarily focused on pyrolysis behavior of CC and CS and products yields [4,13,20–23]. Detailed characterization of biochar produced from CC and CS is still limited. Cao et al. [24] carried out slow pyrolysis of corncob powder under an $N_2$ atmosphere at temperatures of 350-600 °C by using a thermogravimetric analyzer together with mass spectrometry. The yield and composition of gas and liquid products from pyrolysis of corncob powder were characterized. But both the sample size and mass of corncob studied in Cao's work are too small to give indications to practical production processes. In the other work, production of biochar using self-purging and $N_2$ purging reactor was studied and reported by Intani et al [13]. However, the main focus of Intani 's work was to study effect of pyrolysis conditions on biochar yields from corncob. Detailed characterization of the produced biochars were not conducted. The current work aims to fill the knowledge gap regarding characterization of CC and CS biochar with combination of different analytical techniques. The results from this work can be valuable for further assessing and comparing CC and CS biochar with other well studied biochars and identitying proper ways for efficient utilization of them. In addition to the solid biochar, there is also increasing interest to exploit energy contained in the liquid and gases, which are by-product streams from the pyrolysis of biomass materials. One way to realize this is to combust the gas products to generate heat to sustain the pyrolysis process and/or to dry the biomass feedstock [4]. Co-production of char, liquid bio-oil, and non-condensable gases, together with the smart utilization of the last two can improve the material conversion efficiency and energy efficiency of the pyrolysis system [9]. However, very little is known about energy distribution of products generated from the pyrolysis of CC and CS. Study results have been obtained and reported regarding production, characterization and utilization of biochar produced from woody biomasses for different applications [6,9-11]. The results illustrate positive effects and promising roles of wood biochar as applied in different sectors. Due to the distinct chemical compositions and physical characteristics of woody biomass and herbaceous biomass such as CC and CS, the physiochemical properties of biochars produced by slow pyrolysis might be substantially different. Therefore, it is valuable to compare biochars produced from CC, CS, and woody biomass to assess the potential role and performance of CC and CS biochars as used for a certain application.

The current study investigates the pyrolysis behavior of corn cob, corn stalk, and spruce wood and the effect of feedstock on the yield and properties of the produced biochars. A representative pyrolysis temperature of 600 °C was selected for pyrolysis of biomass in a fixed-bed reactor. The temperature was high enough to realize thermal decomposition of the main constitutents in the studied biomass and obtain biochars with comparable physiochemical properties. Biochars produced from the corn cob, corn stalk, and spruce wood were compared based on detailed measurements and analyses of the mass yield, elemental composition, chemical structure, morphology and microstructure, and ash content and composition. Based on the analysis of these results, the utilization of corn cob and corn stalk for biochar production and application was assessed and discussed. Additionally, with mass yield and analyses on main products from the pyrolysis process, energy stored in biochar, liquid and gas products were

investigated, aiming for simultaneous biochar production and use of pyrolysis gases as the energy source for the processes. The results presented in this work can offer valuable insights into the efficient conversion and application of biochar produced from corn residues.

## 2. Biochar production and characterization

### 2.1. Raw feedstock

Corn stalk (CS) and corn cob (CC) were collected from an agricultural field located in Ås, Norway. The collected corn stalk and corn cob were air dried at room temperature for 48 h and then cut into pieces with length of 3-5 cm. The spruce tree was harvested from a forest located in Southern Norway. The stem wood was first debarked and shred into chips with sizes in the range 3–5 cm. The corn stalk, corn cob and spruce wood pieces were then placed in a drying oven at 105 °C for 12 h before pyrolysis campaigns. The milled samples were oven dried at 45 °C for 6 h. For these oven dried samples, Klason and acid-soluble lignins were determined. In brief, 1 g of the sample was mixed with 15 ml of 72% $H_2SO_4$ with reaction time of 2 h. Then the mixture was diluted to 3% $H_2SO_4$, which was further autoclaved at 121℃ for 30 min. The hydrolyzed mixture was filter and solid residues was washed by using deionized water until sulfate ion was undetectable. The washed residues were dried in an oven at 105 °C for measuring weight gravimetrically. The amount of hemicellulose in biomass was determined by solvent extraction. 1 g of sample was mixed with 150 mL of Sodium Hydroxide (NaOH) solution (0.5 mol/L). The mixture was heated to temperature 80℃ for 4 h. Afterwards, the mixture was washed with deionized water until Na+ is nondetectable by using pH paper. The content of cellulose is calculated by difference of the initial weight of sample and weight of lignin, hemicellulose and ash.

### 2.2. Biochar production

Biochar production experiments were carried out in a vertical tubular fixed bed reactor, which was heated by an electrical furnace. For each production experiment, biomass feedstock was loaded in the reactor to form a bed height of about 35 cm. After being loaded with sample, the tubular reactor was placed inside the furnace, sealed and connected with a gas supply system and the condenser. The temperature in the furnace was monitored by three thermocouples located on the top, middle and bottom of the furnace. In addition, one thermocouple inserted into middle of the reactor, monitored the temperature in the center of the sample bed during each biochar production experiment. The sealed tubular reactor was purged with 2 L $min^{-1}$ nitrogen to flush away air before an increase of temperature to generate an inert atmosphere, thereby avoiding possible oxidization and ignition of the solid biochar and produced gases. After purging with nitrogen at room temperature 25 °C for 1 h, the sample was heated up to 600 °C at a nominal heating rate of about 10 °C $min^{-1}$ and kept at the final temperature for 1 h. Then the power supply to the furnace was cut off and the reactor was cooled down to 30 °C with continuous purging of nitrogen. After the reactor was completely cooled down to 30 °C, the biochar was collected and weighed, and then stored for further characterization and testing purposes. The solid product mass yield of one pyrolysis experiment was calculated as the percentage of initially loaded pre-dried biomass sample as follows: $mass\ yield = \left(\frac{m_{dry\ basis\ pyeolyzed\ solid}}{m_{dry\ basis\ feedstock}}\right) x\ 100$. During each biochar production experiment, the volatile products released from the sample were first passed through a condenser. Condensable compounds were cooled down at 5 °C and collected in a metal tank under the condenser. The non-condensable gases were sampled and analyzed online by using a micro-GC (Varian Cp-4900). The micro-GC was equipped with two injectors connected to a chromatographic column individually. The first column was a 10 m PoraPLOT type with using high purity Helium as a carrier gas to measure $CO_2$, $CH_4$, $C_2H_4$ and $C_2H_6$. The second column was a 10 m long Molsieve 5 Å and was purged with Argon. This column was used to separate and measure concentration of $H_2$, $O_2$, $N_2$, $CH_4$ and CO. The non-condensable gas masses were calculated knowing the $N_2$ flow, which was kept constant at 2 L $min^{-1}$. Before one experiment, the Micro GC is calibrated by the external standard method using certified gas containing the target compounds. Standard gas mixtures containing $CH_4$, $C_2H_4$, $C_2H_6$, $H_2$, CO and $CO_2$ with specified concentrations were used for quantitative calibration and helium, ultra-high purity 99.999 - 99.9999% was for use as a carrier gas. Over time, small amounts of contaminants accumulate especially in the column, and can cause peak tailing and retention time shifts. Hence periodic bake out of the column and detector are conducted to optimize the chromatography of the instrument.

The higher heating value of corn cob, corn stalk, biochar and liquid product from pyrolysis experiments were determined by using an IKA C 5000 bomb calorimeter. 0.5 g of dried solid sample was fed into the calorimeter and burned in pure oxygen under 30 bar pressure. The higher heating value of gas products was calculated by the following equations:

$$\mathbf{HHV_{gas}[MJ\,/\,Kg]} = ((\mathbf{m_{H2}xHHV_{H2}}) + (\mathbf{m_{CO}xHHV_{CO}}) + (\mathbf{m_{CH4}xHHV_{CH4}}) + (\mathbf{m_{C2H6}xHHV_{C2H6}}) + (\mathbf{m_{C4H6}xHHV_{C4H6}})/\mathbf{m_{gas}})$$

The calorific value of biochar, liquid product and gases were then used to determine energy distribution.

### 2.3. Biochar characterization

#### 2.3.1. General analysis

Proximate analysis of pre-dried biomasses and produced biochar samples was conducted in accordance with ASTM standard D1762-84. For measuring moisture content the biochar sample of 1 g was placed in a porcelain crucible and dried at 105 °C in a drying oven for 12 h. The dried sample after moisture content measured was loaded in open crucible and heated up to 950 °C in a muffle furnace for 11 min and for ash content 750 °C for 8 h (uncovered crucible). The sample weight differences before and after heating was determined as moisture content, volatile matter content and ash content. The difference between weight of original sample and the sum of moisture content, volatile matter content and ash content corresponds to the fixed carbon content. For each sample, triplicate analyses were conducted and mean values together with standard deviation are reported.

#### 2.3.2. Element analysis

The elemental composition of pre-dried CC and CS and produced biochar samples were analyzed by employing an elemental analyzer (Eurovector EA 3000 CHNS-O Elemental Analyser). Oxygen content of a sample was calculated by difference to avoid interference of inorganic oxides in the ash.

#### 2.3.3. FTIR analysis

Pellets were prepared by mixing 1 mg of finely ground biochar with 150 mg of dry KBr in an agate mortar. The spectra were collected with a FT/IR-6300 Fourier Transform Infrared Spectrometer (JASCO Inc. Japan). For each spectrum a total of 60 scans were collected from 800 to 4000 cm-1 with a resolution of 2 cm-1. The spectra were corrected by using pure KBr as blank as indicated by the spectrometer's JASCO® software.

#### 2.3.4. Inorganic element analysis

Contents of inorganic elements in the pre-dried feedstock and produced biochar were measured using an inductively coupled plasma-atomic emission spectrometer (ICP-AES). Each sample was dissolved in a mixture of acids ($HNO_3$, HF and $H_3BO_3$) and prepared through a pressurized multi-step digestion process. The digested solution was then analyzed by ICP-AES for elemental detection. Triplicate analyses were

conducted for each sample and mean values are reported.

#### 2.3.5. Specific surface area, specific pore volume, and pore size distribution characterization

The pore structure of the produced biochar, including specific surface area, specific pore volume, and pore size distribution, was characterized with $N_2$ and $CO_2$ adsorption. The $N_2$ adsorption isotherms were measured in the relative pressure ($p/p_0$) range of $\sim 5 \cdot 10^{-6}$ to ~1 at 77 K. The $CO_2$ adsorption isotherms were determined in the relative pressure ($p/p_0$) range of $\sim 1 \cdot 10^{-4}$ to $\sim 2.9 \cdot 10^{-2}$ at 273 K. Prior to the adsorption measurements, the biochar samples were milled and degassed in vacuum at 150 °C for at least 8 h. The $N_2$ adsorption measurements were performed in an analyzer Autosorb-1-MP (Quantachrome Instruments, USA). The $CO_2$ adsorption isotherms were obtained in an analyzer Nova 2200 (Quantachrome Instruments, USA). The adsorption data were evaluated with the software NovaWin (Quantachrome Instruments, USA). From the $N_2$ adsorption isotherms, the specific surface area was determined by applying the BET method, the specific pore volume was derived from the total volume of $N_2$ adsorbed at a $p/p_0$ close to 1, and the pore size distribution was characterized by applying the QSDFT (quenched solid density functional theory) method on the adsorption isotherm and considering slit/cylindrical pores. The range of application for the BET method was selected following the recommendations provided by Maziarka et al. [38]. For the three biochars, the upper limit of the $p/p_0$ range for the application of the BET method was below 0.1 [38]. From the $CO_2$ adsorption isotherms, the specific surface area, specific pore volume, and pore size distribution were determined by applying the NLDFT (non-local density functional theory) method on the adsorption isotherm. The true density of the biochar samples was analyzed by using a helium pycnometer (Anton-Paar Ultrapyc 5000). Before the analysis, the samples were milled and dried at 106 °C for 90 min.

#### 2.3.6. Solid state $^{13}C$ Nuclear magnetic resonance (NMR) analysis

Corn cob (CC), corn straw (CS), and spruce wood (SW) biochar samples were analyzed in a 7 mm zirconium oxide rotor in a Bruker DSX 200 spectrometer to obtain $^{13}C$ nuclear magnetic resonance (NMR) spectrum, using cross-polarization magic angle spinning (CP/MAS) technique. The sample was rotated at the magic angle (54.78°) with a spinning speed of 6.8 kHz to avoid line broadening due to orientation-dependent interactions. For each sample the number of scans was set to 10,000 and the delay time was 1.0 s. The $^{13}C$-chemical shifts were calibrated relative to tetramethylsilane (= 0 ppm) with glycine (176.04 ppm). Finally, the spectrum was divided into four different chemical shift regions that were assigned as follows: 0–45 ppm (alkyl C), 45–95 ppm (O/N-alkyl C/ methoxyl C), 95–165 ppm (aryl C + intensity of the spinning side bands), 165–220 ppm (carboxyl & carbonyl C). For quantification, these regions were integrated using MestReNova10® software package for Mass Spectrometry (Mestrelab Research, Santiago de Compostela, Spain).

#### 2.3.7. Scanning electron microscopy (SEM) analysis

The microstructure and morphology of biochar samples were examined by using a scanning electron microscope (Zessia Ultra. 55 Limited Edition). The biochar samples collected from the reactor before and after grinding were examined. To examine more details from the biochar samples before grinding, the following pretreatment and analyses were carried out, including (1) top view scanning of the initial sample, (2) top view scanning on horizontal cross-section area of horizontally sliced sample, and (3) scanning on cross-section area of vertically sliced sample.

**Table 1**
Characteristics of corn stalk, corn cob and spruce wood for biochar production.

| | | Corn stalk (CS) | Corn cob (CC) | Spruce wood (SW) |
|---|---|---|---|---|
| Proximate analysis | | | | |
| Volatile matter content | wt% d. b. | 82.42±0.36 | 82.38±0.15 | 86.6±0.19 |
| Ash content | wt% d. b. | 2.91 ± 0.07 | 5.04 ± 0.04 | 0.22 ± 0.02 |
| Fixed carbon content | wt% d. b. | 14.68±0.36 | 12.45±0.13 | 13.22 ± 0.25 |
| Element analysis | | | | |
| Carbon | wt% d. b. | 43.6±0.45 | 47.4±0.32 | 47.7±0.29 |
| Hydrogen | wt% d. b. | 5.8±0.06 | 5.8±0.03 | 5.7±0.02 |
| Nitrogen | wt% d. b. | 1.1±0.01 | 0.6±0.02 | 0.1±0.01 |
| Sulphur | wt% d. b. | 0.1±0.06 | 0.1±0.07 | 0.0±0.03 |
| Oxygen * | wt% d. b. | 49.4±0.43 | 50.1±0.39 | 46.5±0.27 |
| H/C | | 1.6 | 1.4 | 1.4 |
| O/C | | 0.8 | 0.8 | 0.7 |
| Cellulose | wt% d. b. | 33.6 | 29.6 | 40.1 |
| Hemicellulose | wt% d. b. | 29.7 | 37.9 | 20.3 |
| Lignin | wt% d. b. | 22.9 | 18.5 | 31.1 |
| Ash | wt% d. b. | 2.9 | 5.0 | 0.2 |
| Other | wt% d. b. | 10.9 | 9.0 | 8.4 |
| Inorganic element | | | | |
| K | mg/kg d.b. | 6460.0 | 10610.0 | 1001.5 |
| Ca | mg/kg d.b. | 1510.0 | 390.0 | 896.8 |
| P | mg/kg d.b. | 870.0 | 1590.0 | 63.6 |
| Mg | mg/kg d.b. | 1336.0 | 916.0 | 10.3 |
| S | mg/kg d.b. | 880.0 | 870.0 | 0.3 |
| Si | mg/kg d.b. | 8711.8 | 4139.1 | 109.4 |
| Na | mg/kg d.b. | 625.6 | 273.6 | 99.7 |
| Al | mg/kg d.b. | 2127.0 | 957.0 | 25.8 |
| Zn | mg/kg d.b. | 4.4 | 26.0 | 3.4 |
| Pb | mg/kg d.b. | 2.9 | 0.4 | 0.5 |
| Mn | mg/kg d.b. | 36.0 | 28.0 | 0.4 |
| Fe | mg/kg d.b. | 1102.0 | 657.0 | 3.9 |
| Cu | mg/kg d.b. | 4.7 | 6.7 | 37.8 |

d.b.: dry bas; daf: dry ash free basis.
* Calculated by difference.

## 3. Results

### 3.1. Feedstock

Table 1 shows characteristics of oven dried corn cob (CC), corn straw (CS), and spruce wood (SW) samples. The proximate analysis results show that the CS and CC samples had high content of volatile matter. The ash content of CC was 5.0 wt% and relatively higher than that of CS. The elemental composition of CS and CC were rather similar, with exception of slightly higher nitrogen content for CS. The chemical composition of biomass can be generally characterized by three primary

components including cellulose, hemicellulose and lignin. The absolute amount and chemical structure of cellulose, hemicellulose and lignin differ naturally between biomass materials at various level, i.e., between and within species and between components, which are affected by plant growth conditions and environment stress [25]. As shown in Table 1, CC and CS contained less lignin and cellulose as compared to the SW and had a relatively high content of hemicellulose. The lignin content in woody biomasses is generally higher than those herbaceous biomasses [12]. The lignin content of CS was slightly higher than that of CC. The lignin is more abundant in stem part of crop, which presents hydrophobicity for transporting water and solutes from bottom to top of the plant [26]. As a major cell wall component, lignin is of great importance to provide rigidity and strength of the cell wall and give mechanical support for the plant organs [26]. The major chemical compositions in the biomass material will decompose and interact during pyrolysis process, giving significant impacts on general conversion process and yield and property of final products. As shown in Table 1, both ash content and absolute concentration of inorganic elements in CC and CS were significantly higher than that of SW. It has been reported that inorganic element usually present higher concentrations in herbaceous materials, especially for annual crops [23]. The concentration of P and K in CC were considerably higher than those in CC, which are particularly important at growing points like leaves and grains. On the other hand, Si content in CS was about two times higher than that in CC. The Si in most cereal and crop species forms a silicate network structure and silicate skeleton on the external surface of the stalk/stem, which provides structural strength and protection against microorganism [27]. The alkali earth metals Ca and Mg are also required for plant growth, which occurs largely in the leaves and stem part of the cereal and crop, but with lower concentrations in the seeds and fruits [28]. It partially explains the higher concentrations of the Ca and Mg measured from CS as shown in Table 1.

### 3.2. Product yields

Table 2 shows yield of products from slow pyrolysis of CC, CS and SW. The yields of biochar were similar for CC and CS, which were 25.90% and 26.56%. respectively. It is interesting to note that the biochar yields from slow pyrolysis of CS and CC at 600 °C were comparable or even slightly higher than that of SW. Normally, the yields of biochar from herbaceous biomasses are lower in comparison to those of woody biomasses, since the latter have high bulk density and content of lignin [23]. The condensate yield from pyrolysis of CC was higher than that of CS. Table 2 illustrates that CO and $CO_2$ were the two main components of gas products released from pyrolysis of CC, CS and SW, accounting for 16.65%, 17.33% and 15.16% of the total product yield. In addition, the yield of $CO_2$ from pyrolysis of the three biomasses was nearly three times higher than the CO yield. Compared to SW, the yields of $CO_2$ from CC and CS were higher, which can be partially related to of the higher concentration of hemicellulose in these two biomasses. As shown in Table 1, the content of hemicellulose in CC and CS was 9.7% and 17.9% greater than that in SW, which decompose mainly in the temperature range of 200-400 °C and is the main contributor to $CO_2$ production during the pyrolysis process. In contrast, the yields of CO and $CH_4$ from SW were higher than those from the CC and CS. Product yields from pyrolysis of lignocellulosic biomass can be affected by several factors including absolute and relative concentration of cellulose, hemicellulose ad lignin, reactions between the three components, inherent structures

**Table 2**
Product yields from slow pyrolysis of corn stalk, corn cob and spruce wood.

| | | CS 600 | CC 600 | SW 600 |
|---|---|---|---|---|
| Biochar | wt% d.b. | 25.90 (± 0.6) | 26.56 (± 0.7) | 25.60 (± 0.5) |
| Condensates | wt% d.b. | 55.86 (± 0.2) | 54.46 (± 0.6) | 57.43 (± 0.4) |
| $CO_2$ | wt% d.b. | 12.31 (± 0.2) | 13.12 (± 0.3) | 9.02 (± 0.2) |
| CO | wt% d.b. | 4.34 (± 0.3) | 4.21 (± 0.4) | 6.14 (± 0.2) |
| $CH_4$ | wt% d.b. | 1.06 (± 0.4) | 1.12 (± 0.5) | 1.58 (± 0.2) |
| $H_2$ | wt% d.b. | 0.19 (± 0.1) | 0.16(± 0.3) | 0.08 (± 0.1) |
| $C_2H_2$-$C_2H_4$ | wt% d.b. | 0.10 (± 0.05) | 0.09 (± 0.08) | 0.12 (± 0.04) |
| $C_2H_6$ | wt% d.b. | 0.25 (± 0.04) | 0.28 (± 0.1) | 0.03 (± 0.03) |

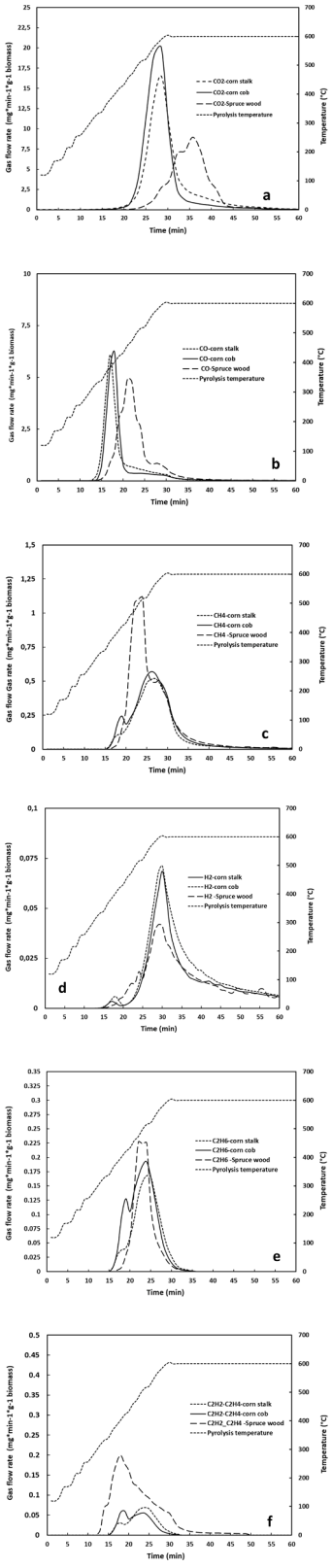


**Fig. 1.** Release profiles gas (a) $CO_2$, (b) CO, (c) $CH_4$, (d) $C_2H_6$, and (f) $C_2H_2$-$C_2H_4$ during pyrolysis of corn cob, corn straw and spruce wood.

and chemical nature of the three components, and effect of biomass structure (i.e., size and density) on these reactions [10,15,6,30]. The differences in the absolute concentrations of three components in the CC, CS and SW possibly account for the different gas product yields obtained in the current work.

Fig. 1 illustrates the release profiles of the main gases $CO_2$, CO, $CH_4$, $H_2$, $C_2H_6$ and $C_2H_2$-$C_2H_4$ produced from pyrolysis of CC, CS and SW. It can be seen that the release intensity of oxygenated gases such as CO and $CO_2$ was considerably higher than $CH_4$ and $H_2$ during the pyrolysis of the studied feedstocks. During pyrolysis of the CC, CS and SW, release of $CO_2$ started from about 250 °C and finished at about 500 °C, which is probably associated with linkages break and dehydration reactions of hemicellulose and initial degradation of cellulose [26]. The profile of CO formation started at temperature about 300 °C and had peaks at temperature of 380 °C, which ended at around 550 °C. Intensive formation of $CO_2$ in the temperature range of 250-500 °C is mainly related to conversion of cellulose and lignin that are the main components of the biomass materials [30]. Fig. 1 shows that the profiles of gas release from CC and CS were similar, and there were clear overlapping peaks of $CO_2$ and CO. However, the release profile of $CO_2$ and CO from SW showed evident differences in comparison to those of CC and CS. In comparison to pyrolysis of CC and CS, the release of $CO_2$ and CO from SW started at higher temperatures about 350 and 380 °C with maximum release values at around 460 °C. This different behavior may be partially attributed to variations in the transport phenomena in the fixed bed. The $CO_2$ and CO release behaviors observed during pyrolysis experiments might be related to both different absolute concentration and chemical structure of hemicellulose and cellulose in of CC, CS and SW. For example, hemicelluloses in woody biomass often constitute $\beta$ (1, 4)-linked glucan, xylan, galactan, mannan, or glucomannan backbone that are branched with single or longer glycosyl residues. Whereas for major cereals, mixed-linkage $\beta$ (1-4):$\beta$ (1-3) glucans and arabino glucuronoxylans are abundant [29]. The compositional and structure property of the three components can undergo their own reaction pathways and actively interact with others during the pyrolysis process [30]. It will influence greatly the overall pyrolysis behaviors of the biomass and yields of products. On the other hand, more significant release of $CH_4$ and $H_2$ was observed from pyrolysis of SW as the temperature was higher than 450 °C. This is associated with rearrangement of the aromatic rings from conversion of lignin in the temperature range of 500- 600 °C[17,18]. In addition, the biomass material was loaded and pyrolyzed in a tubular reactor in the current work, which forms a packed sample bed. The transport phenomena and residence time of the volatiles and gases in the reactor will be different, considering sample bulk density and shape. With different residence time in the reactor, contact time of volatiles and gases with pyrolyzing biomass particles can vary, enabling secondary reactions (both homogeneous and heterogeneous) and different gas release behaviors.

### 3.3. Biochar characterization

#### 3.3.1. Proximate and element analysis

Table 3 summarizes characteristics of CC, CS and SW biochar produced at 600 °C. The volatile matter and ash content varied between biochar derived from CC, CS and SW, which confirms the effects of biomass on the biochar properties. In comparison to the raw feedstock, the volatile matter contents of the produced biochars were considerably lower. The VM/FC ratios of produced biochar samples decreased from 5.8, 6.7 and 6.6 to 0.2, 0.3 and 0.18, respectively. The low VM/FC ratios of the biochars suggest high recalcitrance towards further biological and thermal decomposition. Table 3 also lists the results of element analysis of the produced biochars. The biochar samples presented a carbon content of 73.4%, 79.5% and 86.7%, respectively. Elemental analyses on biochar samples were conducted to calculate the H/C and O/C molar ratio. As shown in the Table 3. the O/C molar ratio of CS biochar was 0.24, whereas for CC and SW biochar was lower. This indicates the latter are more stable and might have half-time of more than 1000 years as claimed and categorized by Spokas et al. [31], which is a great benefit for carbon sequestration. The molar H/C ratio has been used to access the thermochemical alteration degree of biomass and as an indicator of the biochar C structure [32]. The molar H/C ratios of CC and CS biochar were low and comparable with that of SW biochar, indicating high aromaticity and resistance to microbial and chemical degradation.

#### 3.3.2. Inorganic element analysis

Table 4 lists the concentrations of inorganic elements in the produced biochars. K, Ca, P, Mg and Si were dominant elements in the CC and CS biochar, with concentrations significantly higher than those in SW biochar. The CC biochar contained the highest amount of K and P (28410 mg/kg and 4550 mg/kg, respectively), while the highest content in Mg and Si content was detected in CS biochar (6203 mg/kg and 16949 mg/kg). Silicon is usually abundant in the stem part of the crops, especially in rind of stem part, i.e., corn stalk. Silicon has high stability during pyrolysis and retains in the produced biochar, explaining the pronounced high concentration of Si in the corn stalk biochar. P is normally concentrated at the most actively growing points of a plant and stored within seeds in anticipation of their germination [33]. In addition, the calcium content of in the CS biochar was considerably higher compared to that in CC biochar. Calcium is an important element that regulates transportation of other nutrients into the plant from the root to above-ground part, which is particularly active in the root and stem part [2]. Similar high concentrations of K, P, Mg and Ca in the corn stalk biochar were also reported by Intani et al. [13]. The large amount of K and P in the CC and CS biochar suggests they can be promising candidates for soil application with objective of enhancing nutrient content. In addition, biochars with such concentrations of alkali and alkaline earth elements are most likely to have high pH, which can provide a liming effect to soil [34,35]. Corn cob biochar produced at different temperatures have, by others, been tested for amending soil quality,

**Table 3**
Characteristics of biochar produced from corn stalk, corn cob and spruce wood.

| | | CS 600 | CC 600 | SW 600 |
|---|---|---|---|---|
| Proximate analysis | | | | |
| Volatile matter content | wt% d.b. | 15.4±0.31 | 18.3±0.18 | 10.5±0.21 |
| Ash content | wt% d.b. | 9.6±0.02 | 12.4±0.05 | 1.5±0.09 |
| Fixed carbon content | wt% d.b. | 75.0±0.22 | 69.6±0.33 | 88.1±0.23 |
| Element analysis | | | | |
| Carbon | wt% d.b. | 73.4±0.46 | 79.5±0.38 | 86.7±0.29 |
| Hydrogen | wt% d.b. | 1.7±0.21 | 2.2±0.27 | 2.4±0.16 |
| Nitrogen | wt% d.b. | 1.3±0.02 | 0.8±0.04 | 0.1±0.01 |
| Sulphur | wt% d.b. | 0.1±0.12 | 0.1±0.08 | 0.0±0.03 |
| Oxygen * | wt% d.b. | 23.5±0.15 | 17.4±0.17 | 7.7±0.08 |
| H/C | | 0.28 | 0.33 | 0.33 |
| O/C | | 0.24 | 0.16 | 0.07 |

* : calculated by difference

**Table 4**
Inorganic elements in produced corn stalk, corn cob and spruce wood biochar.

| Inorganic element | | CS 600 | CC 600 | SW 600 |
|---|---|---|---|---|
| K | mg/kg d.b. | 21150 | 28410 | 1908 |
| Ca | mg/kg d.b. | 6530 | 1530 | 3298 |
| P | mg/kg d.b. | 3230 | 4550 | 225 |
| Mg | mg/kg d.b. | 6203 | 2564 | 35 |
| S | mg/kg d.b. | 1850 | 1110 | 10.5 |
| Si | mg/kg d.b. | 16949 | 1118 | 398.2 |
| Na | mg/kg d.b. | 918 | 910 | 101.5 |
| Al | mg/kg d.b. | 2107 | 3908 | 50.1 |
| Zn | mg/kg d.b. | 84 | 92 | 102.9 |
| Pb | mg/kg d.b. | 10 | 8 | 4.0 |
| Mn | mg/kg d.b. | 109 | 99 | 0.7 |
| Fe | mg/kg d.b. | 1318 | 2342 | 6.6 |
| Cu | mg/kg d.b. | 28 | 54 | 213.2 |

increasing pH and improving plant crop growth. The results showed soil P and K increased following application of CC biochar, with improvement of soil salinity and pH [36]. Moreover, application of CC biochar was reported to improve soil macro-aggregation and bacterial community structure [37]. It can consequently improve and enhance availability, uptake and use efficiency of the nutrient elements, mainly P and K, with observation of increase of plant tissue K and growth of plants.

### 3.3.3. *Surface area, pore volume, pore size distribution and true density*

The role and performance of biochar in different applications mainly rely on its physicochemical properties. Surface area, pore volume, and pore size distribution are among the most important ones, potentially exerting a vital impact on the performance of biochar in most of applications [38]. During pyrolysis, the decomposition of the carbon matrix and release of volatiles lead to the development of pores (mainly in nm-range) and consequently the formation of the biochar porous structure together with the pores in the μm-range, originating mainly from the parent material. The pores in the nm-range are generally divided into three groups including micropores (pore diameter/width smaller than 2 nm), mesopores (pore diameter/width in the range of 2 to 50 nm), and macropores (pore diameter/width larger than 50 nm), according to the IUPAC classification. To characterize pore specific surface area, specific pore volume, and pore size distribution in the nm range, gas adsorption in a prescribed atmosphere is typically conducted [38]. In the present work, both $CO_2$ adsorption and $N_2$ adsorption was combined, yielding more detailed information about the biochar porosity. Both $CO_2$ and $N_2$ adsorption isotherms for the three biochar samples are presented in Fig. 2. With $CO_2$ adsorption, micropores up to approximately 1.5 nm in diameter are characterized, while $N_2$ adsorption is applied to measure microporosity, mesoporosity, and macroporosity up to around 200 nm in pore size. However, $N_2$ adsorption presents some challenges regarding the characterization of biochar samples dominated by microporosity (especially with small micropores), mainly due to the lower measurement temperature (77 K) and consequent increased intra-particle transport limitations, as well as potential pore deformation, resulting often in an underestimation of biochar microporosity [38–40]. This effect is yet worsened by the complex structure and connectivity that characterizes biochar porosity, especially in the nm-range, as well as by the presence of condensed volatiles and inorganic species on the biochar internal structure, potentially blocking some micropores.

The porosity in the nm-range of the three biochars analyzed in the present work was dominated by micropores (pore diameter/width smaller than 2 nm). This can be seen in the form of the $N_2$ adsorption isotherms (Fig. 2, right), with little to negligible $N_2$ uptake at high relative pressures ($p/p_0$), as well as in the derived pore size distribution (Fig. 3), resulting in negligible specific surface due to mesopores (pore diameter/width in the range of 2 to 50 nm) in comparison to that resulting from micropores. The pore size distribution for micropores yielded by $N_2$ adsorption was not included in Fig. 3, in favor of the pore size distribution resulting from $CO_2$ adsorption. The $N_2$ adsorption results were used to determine the specific surface area distribution according to pore size in the mesoporous region. The values for specific surface area (SSA) and specific pore volume (SPV) resulting from $N_2$ and $CO_2$ adsorption, as well as the material true density (determined with He-pycnometry) for the three biochar samples (SW 600, CS 600, and CC 600) are provided in Table 5. The formation of pores in the nm-range and increase of SSA during pyrolysis of biomass are mainly attributed to the volatilization of organic compounds. The decomposition of hemicellulose and cellulose takes place in the temperature range of 200–400 °C, while lignin has a more complex structure and intricate degradation mechanisms [38]. Decomposition of lignin mainly takes place in the temperature range of 350-500 °C and continues gently up to 900 °C [16,30]. Therefore, dramatic increase in surface area and pore volume in the nm-range mainly occurs in the range of 300-500 °C [16]. At temperatures above 500 °C, the decomposition and devolatilization of biochar is minor; however further restructuring of the solid phase takes place. The development of pores in the nm-range during pyrolysis has been reported to be closely related to the chemical structure and the lignin content of raw biomasses [14,16]. The higher the lignin content of in the biomass feedstock, the greater the biochar surface area and pore volume in the nm-range should be, when produced via slow pyrolysis in the mild temperature range from 350-600 °C [42]. As displayed in the Fig. 1, release of $CH_4$ during pyrolysis of SW was significantly more intensive in the temperature range of 450-500 °C, which continued after the temperature reached 600 °C. This is partially related to degradation of the lignin in the SW. Decomposition of lignin in biomass at a higher temperature often leads to formation of pores and increase in surface area. It can partially explain that SW 600 showed highest porosity (specific surface area and specific pore volume) in the nm-range than CC 600 and CS 600. This biochar also presented the lowest ash content and highest C content. CS 600 and CC 600 biochars showed similar specific surface area and specific pore volume, according to the $CO_2$ adsorption results (Table 1), but lower values in comparison to SW 600. Noteworthy to mention is the larger variability in the $CO_2$-isotherms from CC 600 in comparison to those for CS 600 and SW 600 (larger error bars based on standard deviation, see Fig. 2). Since the three biochars were produced in the same conditions, the differences in porosity in the nm-range are mainly attributed to the different physiochemical properties of parent materials. The high content in lignin of SW may partially explain the higher specific surface area and specific pore volume of the biochar sample SW 600, as previously discussed. However, the different ash content must also be taken into consideration. The pores can be blocked and filled with ash after transformation and migration, particularly for micropores [40]. The blockage of micropores due to migration and sintering of inorganic elements has been observed in biochars from herbaceous biomasses. In a recent review, a survey on biochar produced from a wide range of biomasses showed that biomass with high ash content had lower specific surface area attributed to micropores,

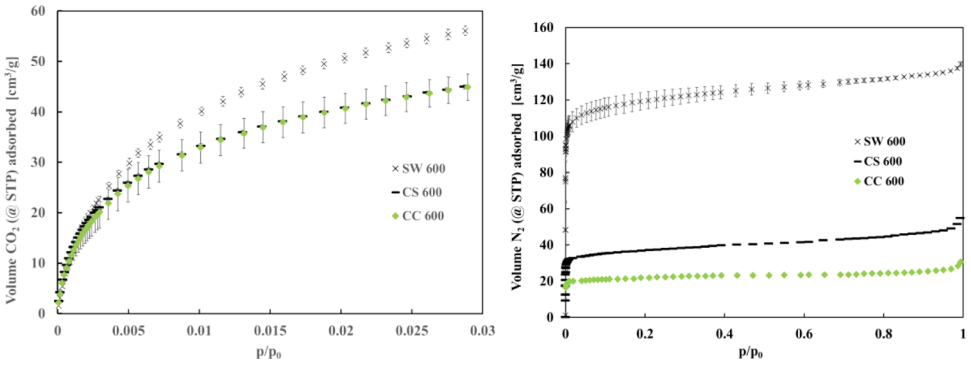


**Fig. 2.** Adsorption isotherms (desorption isotherms not included) for corn stalk, corn cob and spruce wood biochars. Left: $CO_2$ adsorption isotherms. The error bars represent the standard deviation in the measurements. Right: $N_2$ adsorption isotherms.

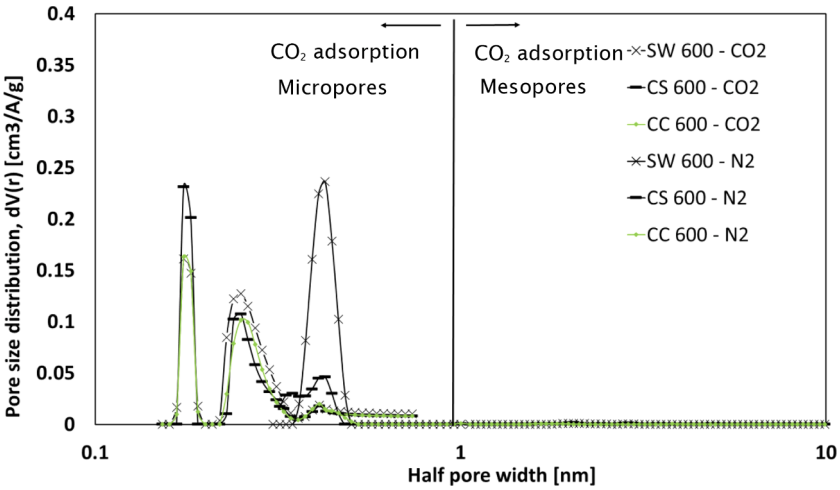


**Fig. 3.** Distribution of specific surface area according to pore size of the corn stalk (CS), corn cob (CC), and spruce wood (SW), derived from the $CO_2$ and $N_2$ adsorption isotherms, after applying the NLDFT and QSDFT methods on the adsorption branches, respectively.

**Table 5**
Specific surface area, specific pores volume, and material density of the produced biochars at 600 °C (CS 600, CC 600, and SW 600).

| Pore structure characterization | | | CS600 | CC600 | SW600 |
|---|---|---|---|---|---|
| Specific surface area ($CO_2$, NLDFT) | SSA | $m^2\ g^{-1}$ | 470.74 ± 6.31 | 477.11 ± 23.13 | 587.53 ± 12.25 |
| Specific pore volume ($CO_2$, NLDFT) | SPV | $cm^3\ g^{-1}$ | 0.126 ± 0.002 | 0.129 ± 0.004 | 0.162 ± 0.004 |
| Specific surface area ($N_2$, BET) | SSA | $m^2\ g^{-1}$ | 140.60 | 94.17 ± 10.15 | 465.14 ± 22.83 |
| Specific pore volume ($N_2$) | SPV | $cm^3\ g^{-1}$ | 0.085 | 0.050 ± 0.004 | 0.216 ± 0.002 |
| Density (He-pycnometry) | D | $g\ cm^{-3}$ | 1.53 | 1.62 | 1.52 |

whereas biomass with low ash content and high organic carbon content (i.e., woody biomass) typically possessed a higher specific surface area [40]. This trend was more evident for biochars produced at temperatures higher than 500 °C [40–42]. With respect to the pore size distribution in the micropore range (derived from $CO_2$ adsorption, see Fig. 3), it is possible to see that the three samples showed qualitatively the same characteristics. The specific surface area distribution with respect to the pore size was concentrated in two regions, with peaks for pore diameter/size of 0.35 and 0.5 nm. The ratio of the specific surface area due to the smallest pores (peaking at around 0.35 nm) to the specific surface area for pores around 0.5 nm was larger for CS 600 and CC 600 in comparison to SW 600. This suggests CS 600 and CC 600 has more smaller pores. The lower specific surface area and specific pore volume observed for $N_2$ adsorption for CS 600 and CC 600 may be attributed to the higher content in inorganic species of these two biochars, influencing the transport of $N_2$ into the smallest pores, either due to pore partial blocking or pore deformation. The three biochars showed negligible mesoporosity, as it can be seen by the negligible specific surface area for pores larger than 2 nm (see Fig. 3). The true density of biochar studied in the current work are listed in Table 5. The density and porosity of biochar affect its mobility in the environment and interaction with the soil hydrologic cycle since material with bulk densities less than water (<1 g $cm^{-3}$) will float [43]. All three produced biochar in the present work had relatively higher density than water, indicating low tendency of them to float under certain hydrologic conditions.

### 3.3.4. NMR analysis

The solid-state $^{13}C$ NMR spectra of produced CC, CS and SW biochar samples are shown in Fig. 4. Similar as carbon structure identified in biochar [15-16], the carbon structure of three biochars were mainly composed of alkyl-C (0–45 ppm), O-alkyl-C (45–90 ppm), aryl-C (95–165 ppm), and carboxylic-C (165–200 ppm). The relative contents of the four carbon groups were quantified using peak area quantification method and results are shown in Table 6. The relative content of aryl-C (95–165 ppm) is in the range of 90-94%, whereas the relative content of

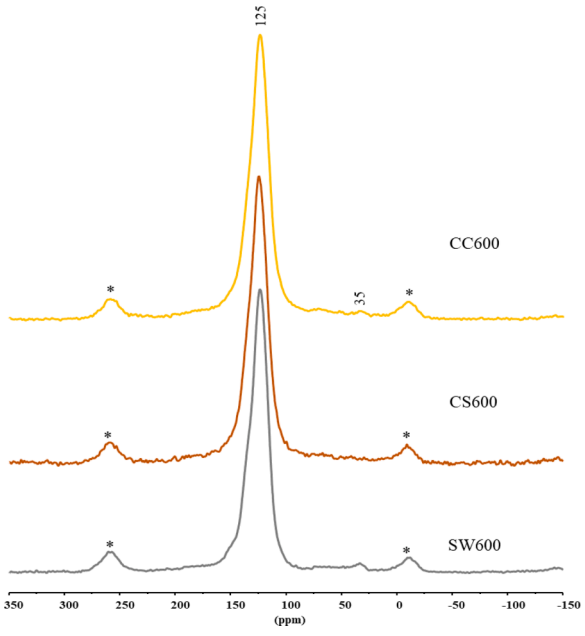


**Fig. 4.** CPMAS $^{13}C$ NMR spectra of corn cob, corn stalk and spruce wood biochar.

carboxyl C fraction are less than 4%, indicating highly aromatic structure of the three biochars (Table 6). Although the structures of CC, CS and SW biochar produced at 600 °C were rather similar, CC600 showed a slightly greater functionality. This is consistent with observations obtained by using solid-state $^{13}C$ NMR spectroscopy and modeled changes for the physical nature of biochar derived from different plant biomasses[14-18]. The ubiquitous peaks at about -10 and 260 ppm are spinning sidebands (SSBs) associated with the aromatic signal. The

**Table 6**
Relative intensity distribution (%) of solid-state $^{13}C$ NMR spectra of corn cob, corn stalk and spruce wood biochar.

| Sample | 0-45 ppm Alkyl-C | 45-95 ppm N-alkyl C/ methoxyl C | 95-165 ppm Aryl C | 165-220 ppm Carboxyl C |
|---|---|---|---|---|
| CC600 | 2 | 4 | 90 | 4 |
| CS600 | 2 | 4 | 91 | 3 |
| SW600 | 2 | 2 | 94 | 2 |

predominance of aromatic C is in a good agreement with several previously published NMR spectra of biochar [44˜46]. It indicates severe condensation and aromatization of biochar both between and within molecules as it is produced a high pyrolysis temperature (i.e., 600 °C). There was also a small peak around 35 ppm, which is related to methylene carbon ($CH_2$). However, the low relative abundance of alkyl-C signals (2%, Table 6) confirmed the high aromaticity of the three biochars. CC and CS biochars also showed some small contribution of O/N-alkyl C (up to 4% of the spectra), which may be derived from surviving ether bonds. The NMR has been recognized as a useful characterization of biochar in terms of stability [44˜45]. The NMR analysis results indicated that the biochars produced in the current work had high aromaticity, and this characteristic will affect their carbon sequestration potential and the duration during which it can provide benefit to the soil.

### 3.3.5. FTIR analysis

The results of the FT-MIR analysis of SW, CC and CS biochar samples are shown in Fig. 5. FT-IR spectra indicated that the three biochars were composed by similar functional groups. The great band width maxima at 1540 $cm^{-1}$ is attributable to the aromatic C═C vibration, possibly formed by heat induced dehydration of cellulose and to aromatic C=O vibrations[47][48]. This signal was shown to decrease with rising temperature by Zhao et al. [42]. The shift of this band in the CS biochar, with a maximum at 1620 $cm^{-1}$, has been attributed as typically indicative for graphite moieties [49,50][ʾ], which is in agreement with the low H/C ratio measured for this sample. However, this signal at CS could also be derived from N-H vibration. All the spectra showed a major band

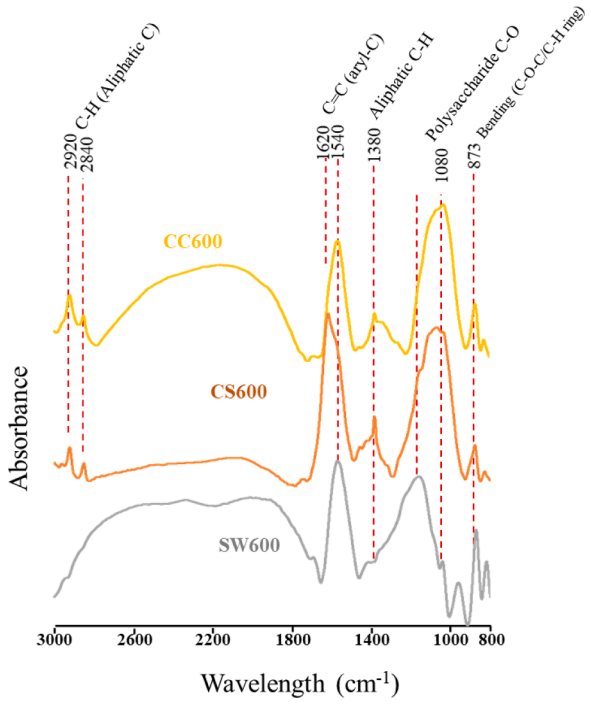


**Fig. 5.** FTIR spectrum of corn cob, corn stalk and spruce wood biochar.

centered at 1080-1085 $cm^{-1}$ which can be caused by C-O stretching vibrations in polysaccharides (cellulose and hemicellulose) or in pyranoses and furanoses derived from of partially converted cellulose and hemicellulose. The peaks at 2920 and 2840 $cm^{-1}$, more evident for CC and CS biochar, correspond to asymmetric $CH_2$ stretching and symmetric $CH_2$ stretching, respectively, and aresigns of remains of aliphatic C [48].

The peak appearing over 1380 $cm^{-1}$ clearly shown in CC and CS biochars, was again correlated with aliphatic groups (-$CH_3$. -$CH_2$. -asymmetric bending), whereas the peak at 873 $cm^{-1}$ could be related to out-of-plane bending of the aromatic ring C-H bonds or $CO_3^{2-}$ bending [51].

### 3.3.6. SEM analysis

Figs. 6–8 show SEM images of CC, CS and SW biochar took from three view directions, which show significant differences could be distinguished between CC, CS and SW in terms of microstructure and morphology. The top three show general view of one scanned biochar grain, and the bottom three are zoom in view with higher magnification to show detailed microstructure of a scanned area. Fig. 6 (a) and (d) display rind layer of the CS biochar, which had a compact and intact surface. The cross section of CS biochar is shown in Fig. 6 (b) and (e) and the latter displays zoom in view of with a higher magnification. The Fig. 6(e) shows the middle part of the corn stalk that consisted of parenchyma tissue and vascular bundles that transport photosynthesis products to the other organs and brings water and salts from underground [33]. Significant differences were found between CC and CS biochar in terms of microstructure as shown in Fig. 7. Fig. 7(a) and (d) show outer chaff part of the scanned corn cob grain, which had a light and stiff wrinkled structure. Fig. 7 (b) and (e) illustrate distinct structural differences between outer woody ring (Fig. 7(b)) and inner pith (Fig. 7(b)). The woody ring had dense structure, which was composed of small size parenchyma structure and vascular bundles. On the other hand, the pith part had spongy honeycomb structure (Fig. 7 e), which is related to preservation of biological capillary structure of corn cob. In comparison to CC and CS biochar, the SW biochar had cellular structure with vertical microchannels and highly elongated tracheids, with observation of longitudinal openings and cracks and pores with different sizes in the cell wall (Fig. 8a and d). Fig. 8b and e display the top view of the vertically cross-sectioned SW biochar, showing it has channel structure and contained both polygonal and elliptical cells. The SEM analyses showed considerably different shapes, densities and physical structures between the produced CC, CS and SW biochar. Such differences indicate variability and structural of three produced biochar, which have recalcitrance and conversion behavior during further applications.

Fig. 9 shows representative SEM images of ground CC, CS and SW biochar used for surface area analysis. As shown in Fig. 9(a), there are large particles greater than 15 μm and small particles that are discrete and aggregated together the large ones. For the larger CC particles, openings and pores with size in the range of 3-10 μm can be observed (indicated with arrows). While for the ground CS biochar, thin flake-like particles can be seen, with openings and pores in similar size around 2-3 μm (indicated with arrows). For the ground SW biochar, in addition to fine flake-like particles, there are some retain tubular structure with spherical pores in the cell wall, which have size in the range of 1-2 μm. The Fig. 9 shows that even after grinding treatment, the biochar can partially persevere structure of parental one and have different microstructure.

## 3.4. Carbon and energy distribution of the products

Recovery and use of by-products is critical to improve efficiency and sustainability and economic profitability of the biochar production process. Considering this, distribution of carbon and energy between products from pyrolysis of the CC, CS and SW were assessed based on

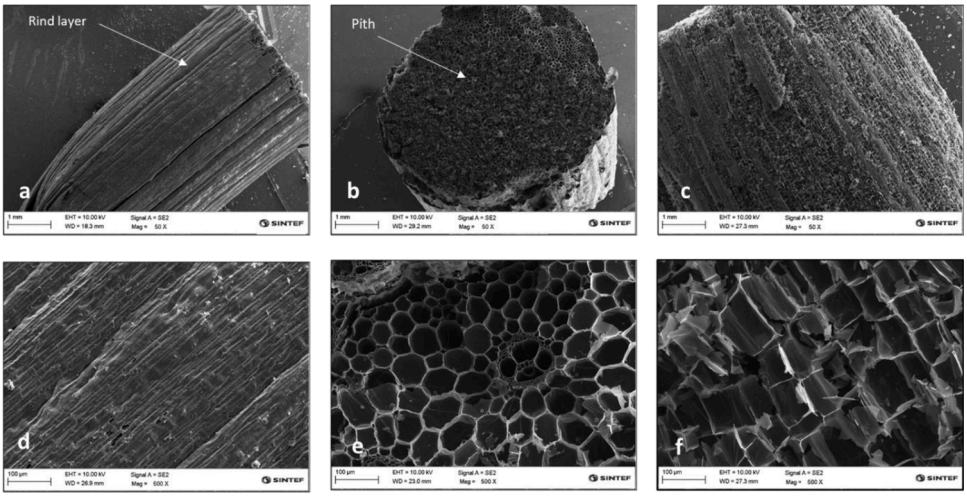


**Fig. 6.** Top view SEM images of (1) surface (a, d), (2) vertically cross sectioned (b, e) and (3) horizontally cross sectioned (c, f) corn stalk biochar.

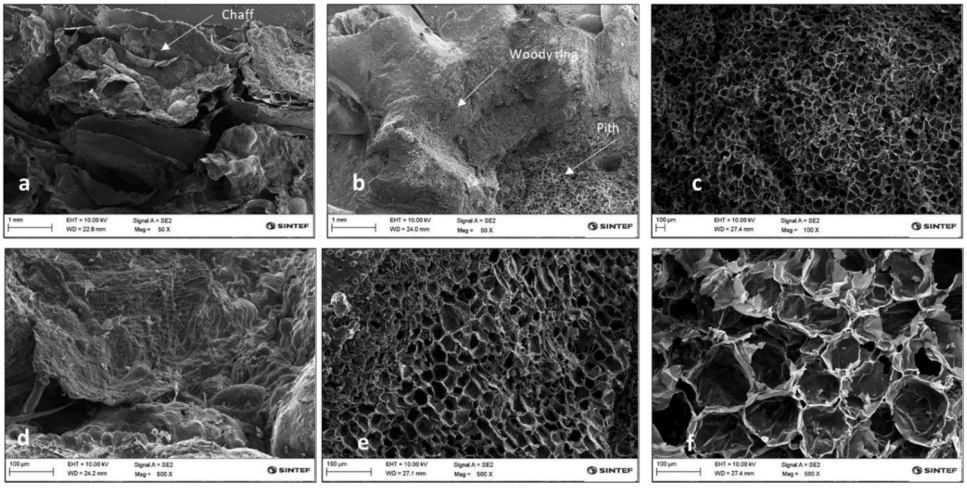


**Fig. 7.** Top view SEM images of (1) surface (a, d), (2) vertically cross sectioned (b, e) and (3) horizontally cross sectioned (c, f) corn cob biochar grain.

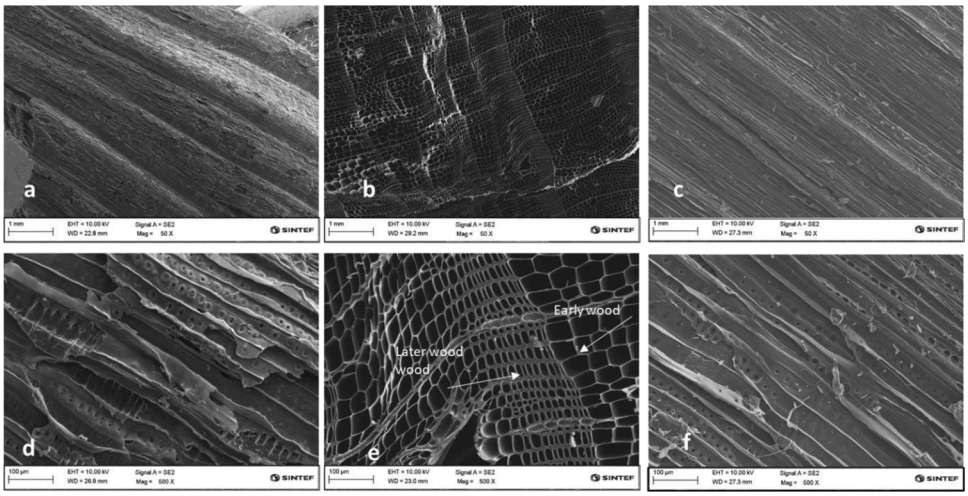


**Fig. 8.** Top view SEM images of (1) surface (a, d), (2) vertically cross sectioned (b, e) and (3) horizontally cross sectioned (c, f) spruce wood biochar grain.

their mass yields, atomic composition and energy content. As shown in Table 7, CS, CC and SW biochar retained over 50% of the carbon in the biomass feedstocks. Effect of feedstock and production conditions on the retainment of carbon in the biochar produced from different biomass materials has been well reported and summarized [5'6'31]. Biochar is a preferred material rich in carbon with highly aromatic carbon skeletons

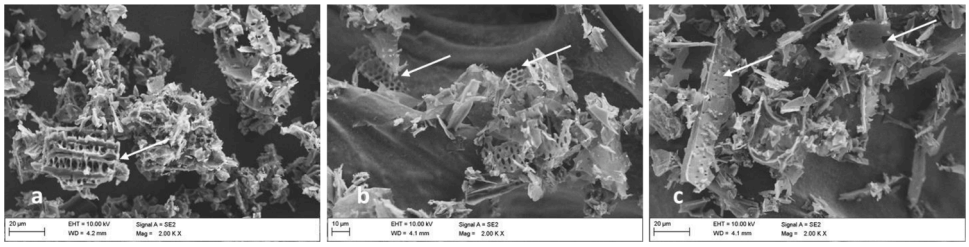


**Fig. 9.** SEM images of ground (a) corn cob, (b) corn stalk and (c) spruce wood biochar.

**Table 7**
Carbon distribution between pyrolysis products from corn stalk, corn cob and spruce wood biomass.

| | CS | CC | SW |
|---|---|---|---|
| Biochar | 61.24 | 60.31 | 56.02 |
| Condensate | 29.00 | 31.02 | 33.88 |
| Gas | 10.13 | 8.94 | 10.21 |

**Table 8**
Energy distribution between pyrolysis products from corn stalk, corn cob and spruce wood biomass.

| | CS | CC | SW |
|---|---|---|---|
| Biochar | 47.72 | 47.99 | 47.47 |
| Condensate | 32.88 | 33.71 | 38.79 |
| Gas | 19.40 | 18.30 | 17.87 |

for carbon sequestration and storage applications [9]. For example, if the CS biochars produced in the current work applied to soil remains without further decomposition, the equivalent $CO_2$ weight can be 69% ($=Y_{biochar}$, wet $\times$ $C_{biochar}$, dry $\times$ 44/12) of the air-dried biomass. This value is comparable with estimated values obtained from studies of biochar from other crop residues [52]. The bio-oil was the second dominant product from biochar production, which had yields of 29.00-33.88% for pyrolysis of CS, CC and SW at 600 °C. As shown in Table 6, the yield of condensates from the CS, CC and SW were rather similar. However, energy content of the condensates produced from SW was higher than those produced from CS and CC. This can be related to different chemical compounds contained in the condensate. The condensates and pyrolytic gases had up to about 38.79% and 19.40% energy yields, when produced from SW and CS, respectively. It is important to note that the by-products of biochar production, condensate and gases, contains over 50% of the energy content compared to that of biochar. Therefore, biochar production can be planned and conducted also considering utilization of by-products as valuable resources.

## 4. Conclusion

In this work, pyrolysis of corn cob, corn stalk, and spruce wood was carried out at 600 °C under inert conditions. The conversion behavior, yields and physico-chemical properties of the biochar products were significantly influenced by the characteristics of the tested biomass feedstocks. Yields of biochar from the CC and CS were comparable with that of SW, which were about 25.90% and 26.56%, respectively. Higher production of $CO_2$ was observed from pyrolysis of CS and CC, which may be related to their greater content in hemicellulose. On the other hand, larger production of CO and $CH_4$ was observed in pyrolysis of SW in comparison to CS and CC, partially due to high content of cellulose and lignin in this woody biomass.

The produced biochars were analyzed via a combination of different analytical techniques. Compared to CS and CC biochars, biochar from SW had a larger surface area in the nm-range, which are favorable for soil application. On the other hand, the CC and CS biochars had evidently high concentrations of inorganic elements (i.e., K and P), which is a desirable property for improving soil fertility. NMR and FTIR analysis results indicated that the biochars produced at 600 °C, irrespective of biomass feedstock, had high aromaticity and stability which suggests greater potential for carbon sequestration application. Condensates and light gases, as by-products from biochar production, contains about 50–60% of energy in total, which are comparable to that of the biochar. Therefore, it is important to assess and utilize the by-products from biochar production as valuable resources for improving carbon and energy conversion efficiency and increasing the economic profitability of the process.

## Declaration of Competing Interest

We declare that we have no financial and personal relationships with other people or organizations that can inappropriately influence our work, there is no professional or other personal interest of any nature or kind in any product, service and/or company that could be construed as influencing the position presented in, or the review of, the manuscript entitled.

## Acknowledgments

This work was fund by The Research Council of Norway through the Project LowImpact (Grant No. 287431/E50) and CARBO-FERTIL (Grant No.281113/E50).

## References

[1] Global corn production from 2014/2015 to 2020/2021. Retrieved from https://www.statista.com/statistics/242632/corn-production-in-china-by-region/.
[2] Li C, Kerner P, Williams CL, Hoover A, Ray AE. Characterization and localization of dynamic cell wall structure and inorganic species variability in harvested and stored corn stover fractions as functions of biological degradation. ACS Sustain Chem Eng 2020;8(18):6924–34. https://doi.org/10.1021/acssuschemeng.9b06977.
[3] He X, Liu Z, Niu W, Yang L, Zhou T, Qin D, Niu Z, Yuan Q. Effects of pyrolysis temperature on the physicochemical properties of gas and biochar obtained from pyrolysis of crop residues. Energy 2018;143:746–56. https://doi.org/10.1016/j.energy.2017.11.062.
[4] Al Afif R, Anayah SS, Pfeifer C. Batch pyrolysis of cotton stalks for evaluation of biochar energy potential. Renew Energy 2020;147:2250–8. https://doi.org/10.1016/j.renene.2019.09.146.
[5] Yuan X, Dissanayake PD, Gao B, Liu WJ, Lee KB, Ok YS. Review on upgrading organic waste to value-added carbon materials for energy and environmental applications. J Environ Manage 2021;296. https://doi.org/10.1016/j.jenvman.2021.113128.
[6] Xie Y, Wang L, Li H, Westholm LJ, Carvalho L, Thorin E, Yu Z, Yu X, Skreiberg Ø. A critical review on production, modification and utilization of biochar. J Anal Appl Pyrolysis 2022;161:105405. https://doi.org/10.1016/j.jaap.2021.105405.
[7] Wang L, Trninic M, Skreiberg Ø, Gronli M, Considine R, Antal MJ. Is elevated pressure required to achieve a high fixed-carbon yield of charcoal from biomass? Part 1: Round-Robin results for three different corncob materials. Energy Fuels 2011;25(7):3251–65. https://doi.org/10.1021/ef200450h.
[8] Wang L, Skreiberg Ø, Van Wesenbeeck S, Grønli M, Antal MJ. Experimental study on charcoal production from woody biomass. Energy Fuels 2016;30(10):7994–8008. https://doi.org/10.1021/acs.energyfuels.6b01039.
[9] Crombie K, Mašek O. Pyrolysis biochar systems, balance between bioenergy and carbon sequestration. GCB Bioenergy 2015;7(2):349–61. https://doi.org/10.1111/gcbb.12137.

[10] Hu X, Gholizadeh M. Biomass pyrolysis: a review of the process development and challenges from initial researches up to the commercialisation stage. J Energy Chem 2019;39:109–43. https://doi.org/10.1016/j.jechem.2019.01.024.

[11] Ronsse F, van Hecke S, Dickinson D, Prins W. Production and characterization of slow pyrolysis biochar: Influence of feedstock type and pyrolysis conditions. GCB Bioenergy 2013;5(2):104–15. https://doi.org/10.1111/gcbb.12018.

[12] L. Williams, R. M. Emerson,J. S. Tumuluru. Book Chapter. Biomass Compositional Analysis for Conversion to Renewable Fuels and Chemicals. doi:10.5772/65777.

[13] Intani K, Latif S, Cao Z, Müller J. Characterisation of biochar from maize residues produced in a self-purging pyrolysis reactor. Bioresour Technol 2018;265:224–35. https://doi.org/10.1016/j.biortech.2018.05.103.

[14] Ma ZQ, Yang YY, Ma Q,Q, Zhou HZ, Luo XP, Liu XH, Wang SR. Evolution of the chemical composition, functional group, pore structure and crystallographic structure of bio-char from palm kernel shell pyrolysis under different temperatures. J Anal Appl Pyrolysis 2017;127:350–9. https://doi.org/10.1016/j.jaap.2017.07.015.

[15] Zhang Y, Ma Z, Zhang Q, Wang J, Ma Q, Yang Y, Luo X, Zhang W. Comparison of the physicochemical characteristics of bio-char pyrolyzed from moso bamboo and rice husk with different pyrolysis temperatures. BioRes 2017;12(3):4652–69.

[16] Ma ZQ, Yang YY, Wu YL, Xu JJ, Peng HH, Liu XH, Zhang WB, Wang SR. In-depth comparison of the physicochemical characteristics of bio-char derived from biomass pseudo components: Hemicellulose, cellulose, and lignin. J Anal Appl Pyrolysis 2019;140:195–204. https://doi.org/10.1016/j.jaap.2019.03.015.

[17] Lee Y, Park J, Ryu C, Gang KS, Yang W, Park Y-K, Hyun S. Comparison of biochar properties from biomass residues produced by slow pyrolysis at 500°C. Bioresour Technol 2013;148:196–201. https://doi.org/10.1016/j.biortech.2013.08.135.

[18] Park Y-K, Yoo ML, Lee HW, Park SH, Jung S-C, Park S-S, Kim S-C. Effects of operation conditions on pyrolysis characteristics of agricultural residues. Renew Energy 2012;42:125–30. https://doi.org/10.1016/j.renene.2011.08.050.

[19] Chen D, Zhou J, Zhang Q. Effects of torrefaction on the pyrolysis behavior and bio-oil properties of rice husk by using TG-FTIR and Py-GC/MS. Energy Fuels 2014;28(9):5857–63. https://doi.org/10.1021/ef501189p.

[20] Zhang X, Zhang P, Yuan X, Li Y, Han L. Effect of pyrolysis temperature and correlation analysis on the yield and physicochemical properties of crop residue biochar. Bioresour Technol 2020;296. https://doi.org/10.1016/j.biortech.2019.122318.

[21] Zhang L, Li S, Li K, Zhu X. Two-step pyrolysis of corncob for value-added chemicals and high quality bio-oil: effects of pyrolysis temperature and residence time. Energy Convers Manage 2018;166:260–7. https://doi.org/10.1016/j.enconman.2018.04.002.

[22] Budai A, Wang L, Gronli M, Strand LT, Antal MJ, Abiven S, Dieguez-Alonso A, Anca-Couce A, Rasse DP. Surface properties and chemical composition of corncob and miscanthus biochars: effects of production temperature and method. J Agric Food Chem 2014;62(17):3791–9. https://doi.org/10.1021/jf501139f.

[23] Panwar NL, Pawar A, Salvi BL. Comprehensive review on production and utilization of biochar. SN Appl Sci 2019;1(2):168. https://doi.org/10.1007/s42452-019-0172-6.

[24] Cao Q, Xie K-C, Bao W-R, Shen S-G. Pyrolytic behavior of waste corn cob. Bioresour Technol 2004;94(1):83–9. https://doi.org/10.1016/j.biortech.2003.10.031.

[25] Worasuwannarak N, Sonobe T, Tanthapanichakoon W. Pyrolysis behaviors of rice straw, rice husk, and corncob by TG-MS technique. J Anal Appl Pyrolysis 2007;78(2):265–71. https://doi.org/10.1016/j.jaap.2006.08.002.

[26] Ana Lourenço and Helena Pereira (2017). Compositional Variability of Lignin in Biomass, Lignin - Trends and Applications, Matheus Poletto, IntechOpen, DOI: 10.5772/intechopen.71208. Available from: https://www.intechopen.com/chapters/57976#B62.

[27] Wang L, Hustad JE, Grønli M. Sintering characteristics and mineral transformation behaviors of corn cob ashes. Energy and Fuels 2012;26:5905–16. https://doi.org/10.1021/ef300215x.

[28] Wang L, Skjevrak G, Skreiberg Ø, Wu H, Nielsen HK, Hustad JE. Investigation on ash slagging characteristics during combustion of biomass pellets and effect of additives. Energy Fuels 2018;32(4):4442–52. https://doi.org/10.1021/acs.energyfuels.7b03173.

[29] Wang S, Dai G, Yang H, Luo Z. Lignocellulosic biomass pyrolysis mechanism: a state-of-the-art review. Prog Energy Combust Sci 2017;62:33–86. https://doi.org/10.1016/j.pecs.2017.05.004.

[30] Yang H, Yan R, Chen H, Lee DH, Zheng C. Characteristics of hemicellulose, cellulose and lignin pyrolysis. Fuel 2007;86(12):1781–8. https://doi.org/10.1016/j.fuel.2006.12.013.

[31] Spokas KA, Novak JM, Stewart CE, Cantrell KB, Uchimiya M, DuSaire MG, Ro KS. Qualitative analysis of volatile organic compounds on biochar. Chemosphere 2011;85(5):869–82. https://doi.org/10.1016/j.chemosphere.2011.06.108.

[32] Leng L, Huang H. An overview of the effect of pyrolysis process parameters on biochar stability. Bioresour Technol 2018;270:627–42. https://doi.org/10.1016/j.biortech.2018.09.030.

[33] Gibson LJ. The hierarchical structure and mechanics of plant materials. J R Soc, Interface 2012;9(76):2749–66. https://doi.org/10.1098/rsif.2012.0341.

[34] Ippolito JA, Cui L, Kammann C, Wrage-Mönnig N, Estavillo JM, Fuertes-Mendizabal T, Fuertes-Mendizabal Cayuela, Maria, Sigua G, Novak J, Spokas K, L Borchard N. Feedstock choice, pyrolysis temperature and type influence biochar characteristics: a comprehensive meta-data analysis review. Biochar 2020;2(4):421–38. https://doi.org/10.1007/s42773-020-00067-x.

[35] Biederman LA, Harpole WS. Biochar and its effects on plant productivity and nutrient cycling: a meta-analysis. GCB Bioenergy 2013;5(2):202–14. https://doi.org/10.1111/gcbb.12037.

[36] Buss W, Bogush A, Ignatyev K, Mašek O. Unlocking the fertilizer potential of waste-derived biochar. ACS Sustain Chem Eng 2022;8:12295–303. https://doi.org/10.1021/acssuschemeng.0c04336.

[37] Wang Y, Ma X, Saleem M, Yang Y, Zhang Q. Effects of corn stalk biochar and pyrolysis temperature on wheat seedlings growth and soil properties stressed by herbicide sulfentrazone. Environ Technol Innov 2022;25:102208. https://doi.org/10.1016/j.eti.2021.102208.

[38] Maziarka P, Wurzer C, Arauzo PJ, Dieguez-Alonso A, Mašek O, Ronsse F. Do you BET on routine? The reliability of N2 physisorption for the quantitative assessment of biochar's surface area. Chem Eng J 2021;418:129234. https://doi.org/10.1016/j.cej.2021.129234.

[39] Dieguez-Alonso A, Funke A, Anca-Couce A, Rombolà AG, Ojeda G, Bachmann J, Behrendt F. Towards biochar and hydrochar engineering-influence of process conditions on surface physical and chemical properties, thermal stability, nutrient availability, toxicity and wettability. Energies 2018;11(3). https://doi.org/10.3390/en11030496.

[40] Bachmann HJ, Bucheli TD, Dieguez-Alonso A, Fabbri D, Knicker H, Schmidt H-P, et al. Toward the standardization of biochar analysis: the COST action TD1107 interlaboratory comparison. J Agric Food Chem 2016;64:513–27. https://doi.org/10.1021/acs.jafc.5b05055.

[41] Leng L, Xiong Q, Yang L, Li H, Zhou Y, Zhang W, Huang H. An overview on engineering the surface area and porosity of biochar. Sci Total Environ 2021;763:144204. https://doi.org/10.1016/j.scitotenv.2020.144204.

[42] Fu P, Hu S, Xiang J, Sun L, Su S, Wang J. Evaluation of the porous structure development of chars from pyrolysis of rice straw: effects of pyrolysis temperature and heating rate. J Anal Appl Pyrolysis 2012;98:177–83. https://doi.org/10.1016/j.jaap.2012.08.005.

[43] Brewer CE, Chuang VJ, Masiello CA, Gonnermann H, Gao X, Dugan B, Davies CA. New approaches to measuring biochar density and porosity. Biomass Bioenergy 2014;66:176–85. https://doi.org/10.1016/j.biombioe.2014.03.059.

[44] McBeath AV, Smernik RJ, Krull ES, Lehmann J. The influence of feedstock and production temperature on biochar carbon chemistry: A solid-state 13C NMR study. Biomass Bioenergy 2014;60:121–9. https://doi.org/10.1016/j.biombioe.2013.11.002.

[45] McBeath AV, Smernik RJ, Schneider MPW, Schmidt MWI, Plant EL. Determination of the aromaticity and the degree of aromatic condensation of a thermosequence of wood charcoal using NMR. Org Geochem 2011;42(10):1194–202. https://doi.org/10.1016/j.orggeochem.2011.08.008.

[46] Ben H, Hao N, Liu Q, Ragauskas AJ. Solid-state NMR Investigation of bio-chars produced from biomass components and whole biomasses. Bioenergy Res 2017;10(4):1036–44. https://doi.org/10.1007/s12155-017-9863-2.

[47] Hossain MK, Strezov V, Chan KY, Ziolkowski A, Nelson PF. Hossain, Strezov, Chan, Ziolkowski, & Nelson, 2011 J Environ Manage 2011;92:223–8.

[48] Spiridon I, Teacă C-A, Bodîrlău R. Structural changes evidenced by FTIR spectroscopy in cellulosic materials after pre-treatment with ionic liquid and enzymatic hydrolysis. BioRes 2011;6(1):400–13.

[49] de la Rosa JM, Paneque M, Miller AZ, Knicker H. Relating physical and chemical properties of four different biochars and their application rate to biomass production of Lolium perenne on a Calcic Cambisol during a pot experiment of 79days. Sci Total Environ 2014;499:175–84. https://doi.org/10.1016/j.scitotenv.2014.08.025.

[50] Francioso O, Sanchez-Cortes S, Bonora S, Roldán ML, Certini G. Structural characterization of charcoal size-fractions from a burnt Pinus pinea forest by FT-IR, Raman and surface-enhanced Raman spectroscopies. J Mol Struct 2011;994(1):155–62. https://doi.org/10.1016/j.molstruc.2011.03.011.

[51] Zhao L, Cao X, Mašek O, Zimmerman A. Heterogeneity of biochar properties as a function of feedstock sources and production temperatures. J Hazard Mater 2013;256-257:1–9. https://doi.org/10.1016/j.jhazmat.2013.04.015.

[52] Park J, Lee Y, Ryu C, Park Y-K. Slow pyrolysis of rice straw: analysis of products properties, carbon and energy yields. Bioresour Technol 2014;155:63–70. https://doi.org/10.1016/j.biortech.2013.12.084.